

Toward Generalizable Deblurring: Leveraging Massive Blur Priors with Linear Attention for Real-World Scenarios

Yuanting Gao^{*§}

Tsinghua University

gaoyt24@mails.tsinghua.edu.cn

Yuandong Pu

SJTU, Shanghai AI Lab

puyuandong@pjlab.org.cn

Shuo Cao^{*}

USTC, Shanghai AI Lab

caoshuo@pjlab.org.cn

Xiaohui Li

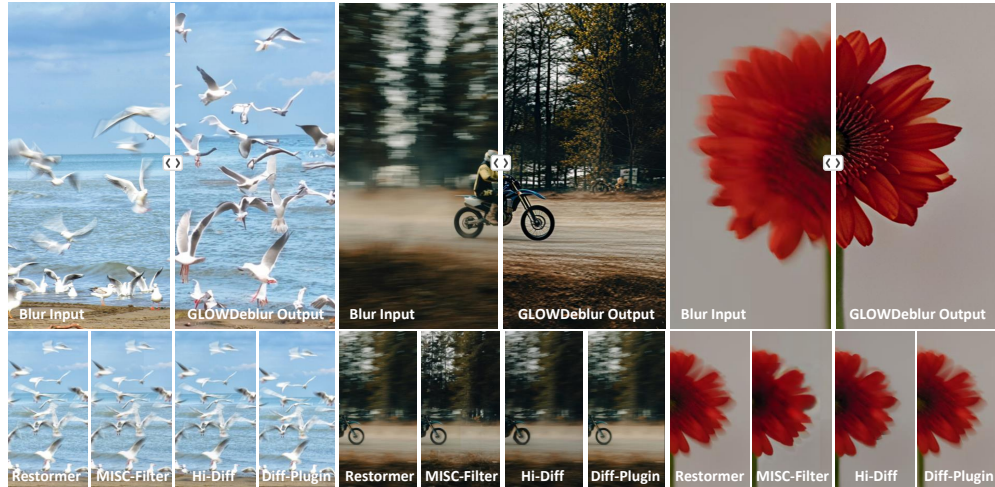
SJTU, Shanghai AI Lab

lixiaohui@pjlab.org.cn

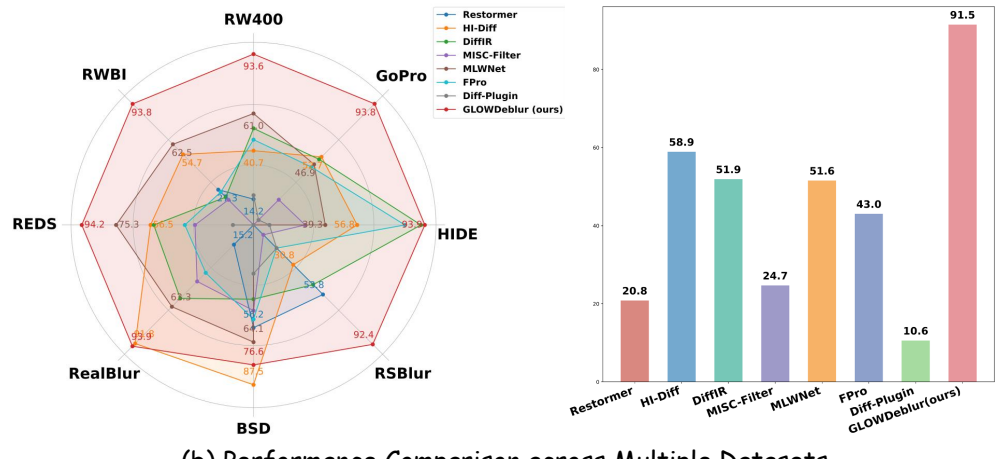
Kai Zhang[†]

Tsinghua University

zhangkai@sz.tsinghua.edu.cn



(a) Deblurring Results on Challenging Real-World Scenes



(b) Performance Comparison across Multiple Datasets

Figure 1. (a) **Visual comparison on challenging real-world images:** our GLOWDeblur effectively restores a wide range of blur patterns, while prior methods often fail in complex scenarios. (b) **Quantitative comparison on diverse benchmarks:** the left plot shows dataset scores computed by ranking methods on each metric and averaging across metrics; the right plot reports average model scores across all datasets, highlighting the strong generalization ability of GLOWDeblur.

*Equal contribution. † Corresponding authors. △Project lead.

§This work was done during his internship at Shanghai AI Laboratory.

Abstract

*Image deblurring has advanced rapidly with deep learning, yet most methods exhibit poor generalization beyond their training datasets, with performance dropping significantly in real-world scenarios. Our analysis shows this limitation stems from two factors: datasets face an inherent trade-off between realism and coverage of diverse blur patterns, and algorithmic designs remain restrictive, as pixel-wise losses drive models toward local detail recovery while overlooking structural and semantic consistency, whereas diffusion-based approaches, though perceptually strong, still fail to generalize when trained on narrow datasets with simplistic strategies. Through systematic investigation, we identify blur pattern diversity as the decisive factor for robust generalization and propose **Blur Pattern Pretraining (BPP)**, which acquires blur priors from simulation datasets and transfers them through joint fine-tuning on real data. We further introduce **Motion and Semantic Guidance (MoSeG)** to strengthen blur priors under severe degradation, and integrate it into **GLOWDeblur**, a **Generalizable realL-wOrld lightWeight Deblur** model that combines convolution-based pre-reconstruction & domain alignment module with a lightweight diffusion backbone. Extensive experiments on six widely-used benchmarks and two real-world datasets validate our approach, confirming the importance of blur priors for robust generalization and demonstrating that the lightweight design of GLOWDeblur ensures practicality in real-world applications. The project page is available at https://vegdog007.github.io/GLOWDeblur_Website/.*

1. Introduction

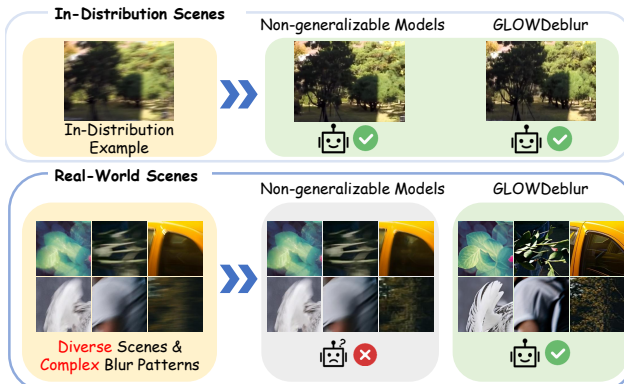


Figure 2. Challenges for Real-World Generalization

In recent years, image deblurring has made significant progress with the rapid development of deep learning. A variety of high-quality datasets [11, 19, 20, 22, 23, 25, 40] and

advanced algorithms [6, 8, 14] have been proposed, achieving impressive performance across benchmarks. However, these advances have not resolved a central limitation: most approaches are trained and evaluated on a limited set of datasets, leading to overfitting to their domain characteristics and specific blur patterns. As a result, their generalization performance drops noticeably when applied to real-world scenarios, where blur is inherently more diverse and complex. As illustrated in Figure 1, where three real-world cases show that current state-of-the-art methods fail to deliver satisfactory restorations not only in complex scenes but also in a visually simple case, reflecting the inherent challenges of real-world blur. Moreover, substantial gaps exist among current datasets, and naive mixed-dataset training not only fails to improve generalization but often degrades performance on the original benchmarks. This raises a central challenge: how to effectively organize existing datasets and design deblurring frameworks that can substantially improve generalization, enabling models to robustly handle the diverse and complex blur patterns encountered in real-world conditions.

Through systematic investigation, we find that this limitation arises from two key aspects: dataset construction and algorithmic design. Current datasets face inherent constraints, making it difficult to achieve both realism and comprehensive coverage of blur patterns. Synthetic datasets such as GoPro [19] and REDS [20] allow large-scale training but diverge from real-world distributions, while real-captured datasets like RealBlur [22] and RSBlur [23] improve realism but remain limited in blur diversity and scene coverage. Even simulation-based datasets such as GS-Blur [11] still differ significantly from real-world degradations. Consequently, substantial gaps remain both across datasets and between synthetic datasets and real-world blur, hindering models trained on a single dataset from achieving robust generalization. Beyond the data, algorithmic choices also impose important constraints. Models trained with pixel-wise losses (e.g., MSE) favor local details but overlook global structure and semantics, leading to smooth outputs with poor generalization [8, 14, 35, 41]. Diffusion models leverage strong priors for perceptually better results, but training on narrow datasets with simple strategies limits their ability to capture diverse blur patterns [6, 15, 30].

Based on these observations, we first conduct a systematic analysis of dataset biases in deblurring. While prior research has largely emphasized the realism of blur [22, 23, 40], we find that the diversity and coverage of blur patterns—such as their orientation and spatial distribution—are critical factors behind the gaps observed both across datasets and between datasets and real-world blur. Motivated by this finding, we propose **BPP (Blur Pattern Pretraining)**: a data-centric strategy where models are first pretrained on large-scale simulation datasets with comprehensive blur patterns, enabling them to learn robust priors that generalize to real-world scenarios.

hensive blur patterns to acquire strong blur priors, and are then jointly fine-tuned on real-captured datasets. This process enables the model to leverage blur priors to bridge dataset gaps, ultimately improving both robustness and applicability in real-world deblurring.

In terms of algorithm design, diffusion models offer strong prior modeling and the ability to integrate heterogeneous data sources, making them well suited for generalizable deblurring. However, their high complexity and resource demands hinder deployment in real-world applications that require real-time efficiency, such as autonomous driving and mobile photography. To address this, we propose **GLOWDeblur**, a Generalizable reaL-wOrld lightWeight **Deblur** model that combines a convolution-based pre-reconstruction & domain-alignment module with a lightweight diffusion model, which employs a Deep Compression AutoEncoder and Linear Attention. To further strengthen the model’s ability to handle diverse and complex real-world blur, we incorporate motion guidance and cross-modal semantic captions as complementary signals, enabling the model to better adapt to varied blur patterns and recover severely degraded regions by leveraging the generative capacity of diffusion models. GLOWDeblur is trained with our Blur Pattern Pretraining (BPP) strategy and extensively evaluated on six widely used benchmarks and two real-world datasets. Since our work targets perceptual quality in diverse real-world blur, we employ a broad set of perceptual-oriented metrics, consistent with recent trends [4, 12, 33, 34] emphasizing visual fidelity beyond pixel-wise accuracy. Results show that GLOWDeblur achieves superior cross-dataset and real-world generalization, underscoring blur priors as the key to real-world deblurring.

In this paper, we present the following contributions:

Revealing the role of blur patterns. We systematically analyze dataset biases and reveal that the diversity and coverage of blur patterns, rather than realism alone, are the decisive factors behind cross-dataset gaps. Learning blur priors and leveraging them as guidance is shown to be essential for achieving robust and quantifiable generalization.

Data and model level priors for generalization. We introduce Blur Pattern Pretraining (BPP), a data-centric strategy that first learns blur priors from large-scale simula-

tion datasets and then jointly fine-tunes on real-captured datasets. In parallel, we propose Motion and Semantic Guidance (MoSeG) to reinforce blur priors and alleviate structural and semantic degradation under severe blur.

A generalizable real-world deblurring model. We propose GLOWDeblur, a diffusion-based framework that balances efficiency and effectiveness, achieving strong performance across six benchmarks and two real-world datasets. Beyond results, it also serves as a practical testbed to validate our insights and demonstrate real-world applicability.

2. Motivation

2.1. Limitations of Existing Models in Real-World Blur Scenarios

Although recent methods have achieved remarkable progress, they still exhibit fundamental limitations, particularly in generalizing to diverse real-world blur patterns. As illustrated in Figure. 1, across three representative real-world scenes, current state-of-the-art methods fail to deliver satisfactory restorations beyond the training distribution, not only under complex scenes but even in visually simple ones. Figure. 2 further reinforces this observation: although existing methods handle in-distribution blur reasonably well, they suffer severe failures when confronted with the diverse and complex scenes and blur patterns of real-world scenarios. This indicates that current approaches rely heavily on dataset-specific distributions rather than learning transferable representations of blur.

These observations motivate us to examine the roots of the generalization gap, revealing that explicitly modeling blur-pattern priors and organizing training data to capture their diversity are crucial for robust real-world deblurring. Guided by these insights, we design improved training strategies and a lightweight model that generalize effectively across diverse scenes and blur patterns (Figure. 2 GLOWDeblur), thereby overcoming the limitations of existing methods.

2.2. Dataset Bias and Blur Pattern Discrepancies

To understand the generalization gap, we conducted a series of cross-dataset experiments using Restormer as a representative backbone. Models were first trained individually on six widely used datasets and one simulation-based dataset

Table 1. Cross-dataset results (PSNR/SSIM) reveal severe generalization gaps, with **red** indicating the best in-dataset and **blue** the second-best cross-dataset result. Avg. column reports mean PSNR/SSIM across datasets.

Training Set \ Test Set	GoPro [19]	HIDE [25]	REDS [20]	RealBlur [22]	BSD [40]	RSBlur [23]	GSBlur [11]	Avg.
GoPro (Synthetic)	32.92 / 0.94	31.22 (↓0.40) / 0.92	26.93 (↓7.46) / 0.82	28.96 (↓1.13) / 0.88	24.43 (↓9.32) / 0.90	29.30 (↓3.68) / 0.86	24.94 (↓6.43) / 0.82	28.39 / 0.88
HIDE (Synthetic)	32.60 (↓0.32) / 0.94	31.62 / 0.93	26.68 (↓7.71) / 0.83	27.76 (↓4.33) / 0.86	25.34 (↓8.41) / 0.85	27.77 (↓5.21) / 0.83	23.40 (↓7.97) / 0.80	27.88 / 0.86
REDS (Synthetic)	26.21 (↓6.71) / 0.83	24.42 (↓7.20) / 0.80	34.39 / 0.94	28.72 (↓3.37) / 0.86	28.90 (↓4.85) / 0.84	28.09 (↓4.89) / 0.87	24.42 (↓6.95) / 0.80	27.88 / 0.85
RealBlur (Real)	24.50 (↓8.42) / 0.82	23.60 (↓8.02) / 0.81	25.85 (↓8.54) / 0.79	32.09 / 0.92	28.78 (↓4.97) / 0.91	29.65 (↓3.33) / 0.87	24.92 (↓6.45) / 0.81	27.06 / 0.85
BSD (Real)	27.27 (↓5.65) / 0.86	26.27 (↓5.35) / 0.85	28.20 (↓6.19) / 0.84	29.64 (↓2.45) / 0.89	33.75 / 0.96	30.45 (↓2.53) / 0.89	26.78 (↓4.59) / 0.85	28.91 / 0.88
RSBlur (Real)	27.55 (↓5.37) / 0.87	25.79 (↓5.83) / 0.84	28.08 (↓6.31) / 0.84	30.41 (↓1.68) / 0.89	30.85 (↓2.90) / 0.94	32.98 / 0.93	27.63 (↓3.74) / 0.86	29.04 / 0.88
GSBlur (Simulated)	28.51 (↓4.41) / 0.90	26.12 (↓5.50) / 0.87	30.29 (↓4.10) / 0.90	30.06 (↓2.03) / 0.91	31.24 (↓2.51) / 0.94	32.01 (↓0.97) / 0.92	31.37 / 0.92	29.94 / 0.91

constructed via 3D Gaussian Splatting, and then evaluated across all datasets. As shown in Table. 1, models trained on one dataset degrade notably on others, underscoring a substantial cross-dataset distribution gap.

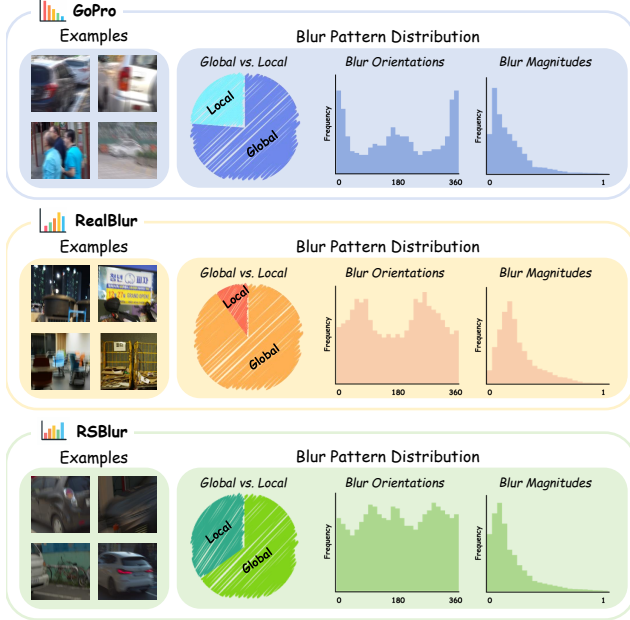


Figure 3. Illustration of dataset-specific blur patterns, highlighting notable distribution differences.

Importantly, Our cross-dataset experiments further reveal two important observations. First, these gaps exist not only between synthetic and real datasets, but also within the same category (synthetic vs. synthetic or real vs. real), indicating that beyond realism there exist deeper sources of mismatch. Second, despite limited realism in both scenes and blur in GSBlur, its broad coverage of blur patterns allows models trained on it to achieve relatively stronger cross-dataset robustness. Collectively, these results highlight that blur pattern diversity, insufficiently recognized in prior work, plays a dominant role in causing the significant cross-dataset gap.

To validate this insight, we conducted a fine-grained analysis of blur characteristics across datasets. As shown in Figure. 3, their blur patterns differ markedly in orientation, magnitude, and locality. In particular, GoPro is dominated by horizontal blur while RealBlur is primarily vertical, yet prior work has often attributed their discrepancy only to differences in realism.

In summary, our analysis shows that dataset bias in deblurring arises primarily from blur pattern mismatches, thereby motivating our exploration of both data-centric strategies to mitigate cross-dataset gaps and algorithmic frameworks that exploit blur priors for robust real-world generalization.

3. Methodology

3.1. Blur Pattern Pretraining (BPP)

Since blur pattern diversity is pivotal for generalization, we propose Blur Pattern Pretraining (BPP), which utilizes datasets with broad blur coverage to enable models to learn intrinsic blur priors, thereby mitigating distribution gaps and enhancing both performance and generalization. Table. 2 empirically validates the effectiveness of this strategy using Restormer as a testbed. Specifically, in settings (a), (b), and (c), applying BPP on a dataset with diverse blur patterns prior to fine-tuning on target real-world datasets (RealBlur, BSD, and RSBlur) consistently yields superior in-distribution accuracy and cross-domain robustness compared to direct training. Furthermore, the comparison reveals the pitfalls of naïve mixed training (d); simply combining datasets fails to achieve optimal results and even degrades performance due to significant domain shifts and conflicting distributions. In contrast, strategy (e) demonstrates that BPP serves as a critical bridge—effectively harmonizing these gaps before mixing, which results in comprehensive improvements across all benchmarks.

Given the demonstrated efficacy of BPP in bridging distribution gaps, we integrate this strategy into the training framework of GLOWDeblur. As illustrated in Figure. 4, the training process consists of two stages: the model first undergoes BPP on a simulated dataset featuring extensive blur coverage to internalize essential blur knowledge and priors. Subsequently, the model is fine-tuned on multiple real-world datasets, adapting these learned priors to realistic degradations to maximize both generalization capability and restoration quality.

3.2. Motion and Semantic Guidance (MoSeG)

While BPP equips models with transferable blur priors, challenges remain under severe or highly diverse blur, where structural cues are ambiguous and low-level details are heavily lost. To address this, we introduce Motion and Semantic Guidance (MoSeG), a conditional design that explicitly reinforces blur priors during inference and training.

Motion Guidance (MoG): To strengthen the guidance of blur priors, we integrate a motion estimation module. Estimation of motion trajectories provides a direct way to characterize blur patterns and enhance the model’s ability to generalize across diverse degradations. The blur can be modeled as the accumulation of displaced sharp pixels along estimated trajectories:

$$B(p_0) = \frac{1}{N} \sum_{n=0}^{N-1} L_s(p_0 + \Delta P_{t_n}), \quad (1)$$

where L_s is the latent sharp image and ΔP_{t_n} the motion offset at t_n .

Table 2. Performance comparison (PSNR/SSIM) on RealBlur-J, BSD, and RSBlur. Settings (a)-(c) validate BPP’s gains in accuracy and robustness. Furthermore, comparing (d) and (e) shows BPP resolves the domain conflicts of naïve mixed training, ensuring comprehensive improvements.

No.	Training set	BPP	RealBlur-J [22]	BSD [40]	RSBlur [23]
(a)	RealBlur	✓	32.26 ($\uparrow 0.17$) / 0.93 ($\uparrow 0.01$)	29.76 ($\downarrow 3.99$) / 0.92 ($\downarrow 0.04$)	30.28 ($\downarrow 2.70$) / 0.89 ($\downarrow 0.04$)
(b)	BSD	✓	29.95 ($\downarrow 2.14$) / 0.90 ($\downarrow 0.02$)	34.21 ($\uparrow 0.46$) / 0.96 (± 0.00)	31.15 ($\downarrow 1.83$) / 0.90 ($\downarrow 0.03$)
(c)	RSBlur	✓	30.63 ($\downarrow 1.46$) / 0.90 ($\downarrow 0.02$)	31.22 ($\downarrow 2.53$) / 0.95 ($\downarrow 0.01$)	33.69 ($\uparrow 0.71$) / 0.94 ($\uparrow 0.01$)
(d)	RealBlur + BSD + RSBlur	✗	30.83 ($\downarrow 1.26$) / 0.89 ($\downarrow 0.03$)	31.99 ($\downarrow 1.76$) / 0.95 ($\downarrow 0.01$)	31.24 ($\downarrow 1.74$) / 0.90 ($\downarrow 0.03$)
(e)	RealBlur + BSD + RSBlur	✓	32.11 ($\uparrow 0.02$) / 0.93 ($\uparrow 0.01$)	33.62 ($\downarrow 0.13$) / 0.96 (± 0.00)	33.65 ($\uparrow 0.67$) / 0.94 ($\uparrow 0.01$)
Best same-dataset performance		—	32.09 / 0.92	33.75 / 0.96	32.98 / 0.93

Following prior work on motion offset estimation [39], we adopt a lightweight encoder-decoder that extracts hierarchical features and predicts dense motion fields ΔP . These offsets are concatenated with blurred-image features and fed into the deblurring network as motion cues.

Semantic Guidance (SeG): In severely blurred regions where structural details are lost, we inject high-level semantics as conditional signals to unleash the cross-modal capacity of diffusion models. Specifically, using Qwen2.5-VL-7B [2], we generate detailed captions describing objects, scenes, context, and other high-level attributes, and feed their embeddings into Linear DiT blocks, enabling the recovery of heavily degraded regions.

3.3. Lightweight Pre-Aligned Linear Diffusion Framework

Real-world deblurring applications, ranging from autonomous driving to mobile photography, demand models that are both highly efficient and compact. To this end, we design a lightweight framework that integrates a Pre-Reconstruction & Domain-Alignment module with a Deep Compression AutoEncoder and Linear DiT blocks, achieving both efficiency and strong performance.

Pre-Reconstruction & Domain-Alignment module: a conventional UNet architecture that provides coarse restoration and aligned intermediate representations, reducing the

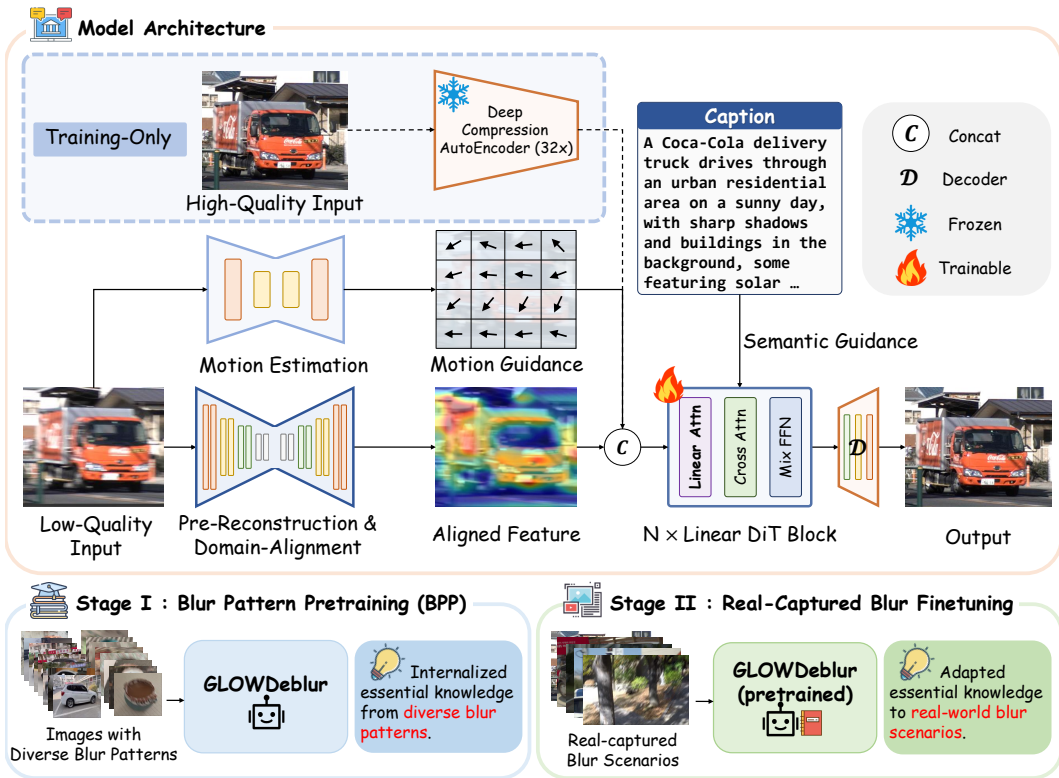


Figure 4. Overview of GLOWDeblur. The framework integrates a Pre-Reconstruction & Domain-Alignment module with a lightweight diffusion framework, guided by motion maps and cross-modal text semantics. Training involves pre-training on datasets with diverse blur patterns, followed by joint fine-tuning on real-captured datasets.

burden on the diffusion backbone. To keep the design lightweight, we follow the philosophy of [5], simplifying architectures with two key modifications. First, nonlinear activations such as GELU are replaced with a SimpleGate, where feature maps are split and fused via element-wise product:

$$\text{SimpleGate}(X, Y) = X \odot Y, \quad (2)$$

preserving gating capacity at negligible cost. Second, channel attention is reformulated as Simplified Channel Attention (SCA), which aggregates global context through pooled descriptors and reweights channels without redundant nonlinearities:

Table 3. Quantitative comparison with state-of-the-art deblurring methods on six widely used benchmarks. Higher values indicate better performance for \uparrow metrics, and lower values for \downarrow .

Dataset	Metrics	Restormer* [35]	HI-Diff [6]	DiffIR [30]	MISC-Filter [14]	MLWNet [8]	FPro [41]	Diff-Plugin [15]	Ours
GoPro [19]	PSNR \uparrow	33.07	33.33	33.20	34.10	24.60	33.05	25.64	25.21
	SSIM \uparrow	0.943	0.964	0.963	0.969	0.83	0.943	0.793	0.787
	MANIQA [32] \uparrow	0.353	0.492	0.535	0.458	0.497	0.518	0.346	0.538
	LIQE [38] \uparrow	1.455	1.350	1.589	1.172	1.353	1.491	1.092	1.502
	NRQM [16] \uparrow	4.748	5.047	5.051	4.339	4.750	4.915	3.886	5.252
	CLIP-IQA [27] \uparrow	0.243	0.250	0.258	0.214	0.257	0.250	0.190	0.239
	PI [3] \downarrow	5.308	5.159	5.135	5.464	5.363	5.151	6.202	4.846
	BRISQUE [17] \downarrow	46.715	46.418	46.721	46.095	49.638	49.121	51.018	39.732
	NIQE [18] \downarrow	5.534	5.504	5.466	5.461	5.650	5.377	6.146	5.120
	ILNIQE [37] \downarrow	33.354	32.710	33.408	33.071	32.535	32.701	42.474	26.464
HIDE [25]	PSNR \uparrow	31.81	31.46	31.55	31.66	23.95	30.70	23.95	24.12
	SSIM \uparrow	0.933	0.945	0.947	0.946	0.819	0.921	0.763	0.763
	MANIQA \uparrow	0.453	0.535	0.592	0.498	0.509	0.572	0.362	0.583
	LIQE \uparrow	1.113	1.621	1.977	1.236	1.392	1.803	1.061	1.788
	NRQM \uparrow	3.916	5.613	6.104	4.731	5.129	6.028	4.323	6.210
	CLIP-IQA \uparrow	0.187	0.227	0.229	0.179	0.224	0.215	0.158	0.212
	PI \downarrow	6.302	4.837	4.354	5.278	5.085	4.308	5.773	4.244
	BRISQUE \downarrow	52.830	43.605	41.045	45.919	48.277	42.970	40.716	36.687
	NIQE \downarrow	6.558	5.254	4.803	5.318	5.348	4.624	5.528	4.673
	ILNIQE \downarrow	36.248	31.246	29.788	29.985	30.702	28.224	40.744	24.176
REDS [20]	PSNR \uparrow	34.207	25.760	26.78	27.58	27.60	26.96	26.27	26.21
	SSIM \uparrow	0.938	0.779	0.819	0.832	0.851	0.840	0.771	0.770
	MANIQA \uparrow	0.536	0.630	0.626	0.607	0.647	0.613	0.518	0.642
	LIQE \uparrow	1.435	2.530	2.293	2.065	2.664	2.097	1.520	2.570
	NRQM \uparrow	4.886	6.849	7.014	6.541	6.954	6.809	6.384	7.352
	CLIP-IQA \uparrow	0.271	0.305	0.287	0.268	0.322	0.269	0.228	0.351
	PI \downarrow	5.335	3.379	3.391	3.546	3.293	3.481	4.160	3.035
	BRISQUE \downarrow	43.364	28.061	26.452	30.115	31.448	28.533	27.867	25.695
	NIQE \downarrow	5.660	3.899	3.973	3.894	3.851	3.966	4.620	3.694
	ILNIQE \downarrow	29.305	23.784	23.269	23.083	22.369	23.236	27.088	19.357
RealBlur-J [22]	PSNR \uparrow	31.131	29.15	25.37	33.88	33.84	27.90	26.25	27.55
	SSIM \uparrow	0.917	0.890	0.825	0.938	0.941	0.873	0.79	0.811
	MANIQA \uparrow	0.472	0.629	0.571	0.602	0.615	0.544	0.467	0.613
	LIQE \uparrow	2.356	2.646	1.949	2.386	2.578	1.735	1.243	2.439
	NRQM \uparrow	5.150	5.870	5.517	5.365	5.685	5.361	4.283	5.633
	CLIP-IQA \uparrow	0.262	0.279	0.247	0.251	0.274	0.212	0.208	0.274
	PI \downarrow	5.235	4.651	4.934	5.011	4.869	5.013	5.965	4.787
	BRISQUE \downarrow	49.636	46.799	40.207	46.610	48.970	42.742	42.401	35.895
	NIQE \downarrow	5.708	5.182	5.258	5.341	5.370	5.256	5.963	5.128
	ILNIQE \downarrow	34.999	33.380	31.848	34.550	33.588	32.580	37.317	27.548
BSD [40]	PSNR \uparrow	30.410	28.66	27.97	29.53	28.82	26.64	27.67	29.56
	SSIM \uparrow	0.923	0.907	0.885	0.923	0.910	0.885	0.862	0.893
	MANIQA \uparrow	0.571	0.565	0.362	0.510	0.536	0.461	0.427	0.568
	LIQE \uparrow	2.325	2.452	1.048	1.742	2.132	1.479	1.296	2.348
	NRQM \uparrow	4.927	5.806	4.634	4.772	5.229	5.141	4.433	5.096
	CLIP-IQA \uparrow	0.279	0.283	0.188	0.234	0.264	0.179	0.195	0.282
	PI \downarrow	5.800	5.189	6.100	5.819	5.560	5.934	6.422	5.589
	BRISQUE \downarrow	47.363	39.518	24.113	46.358	46.388	29.108	36.347	40.514
	NIQE \downarrow	5.799	5.464	6.469	5.758	5.721	5.881	6.569	5.455
	ILNIQE \downarrow	42.040	38.708	31.513	41.328	40.506	37.435	50.182	39.383
RSBlur [23]	PSNR \uparrow	29.27	29.47	22.48	29.98	30.91	26.19	27.82	28.85
	SSIM \uparrow	0.864	0.875	0.651	0.887	0.818	0.833	0.821	0.820
	MANIQA \uparrow	0.442	0.452	0.362	0.420	0.415	0.398	0.441	0.533
	LIQE \uparrow	1.342	1.124	1.048	1.069	1.111	1.018	1.015	1.404
	NRQM \uparrow	3.769	3.817	4.634	3.523	3.642	5.520	4.357	5.597
	CLIP-IQA \uparrow	0.262	0.246	0.188	0.204	0.248	0.170	0.169	0.236
	PI \downarrow	6.427	6.851	6.100	6.820	7.065	6.296	6.677	4.980
	BRISQUE \downarrow	52.768	50.286	24.113	54.119	58.433	39.250	21.942	30.677
	NIQE \downarrow	6.522	7.348	6.469	6.943	7.532	7.533	6.840	5.292
	ILNIQE \downarrow	32.349	37.794	31.513	36.354	39.651	36.035	41.705	25.833

$$SCA(X) = X \odot W_{pool}(X). \quad (3)$$

Together, these modifications substantially reduce computation while retaining representational power.

Lightweight Diffusion with Deep Compression AutoEncoder and Linear Attention: Latent diffusion operates by compressing images into a latent space via an AutoEncoder and applying a DiT for diffusion within this space, where the computational cost is largely influenced by the compression ratio and the complexity of attention mechanisms. To meet real-world efficiency demands, we adopt lightweight adaptations inspired by [12, 31].

While mainstream designs typically adopt an $8 \times$ AutoEncoder for latent compression, we employ a more aggressive $32 \times$ Deep Compression AutoEncoder. With sufficient performance maintained, this design reduces the number of tokens and significantly lowers memory and computation.

Traditional Diffusion Transformers (DiTs) adopt the standard softmax attention mechanism with quadratic complexity $O(N^2)$, which is computationally expensive. we further replace the quadratic self-attention in the DiT with a linear variant, reducing the complexity to $O(N)$.

Given query $\mathbf{Q} \in \mathbb{R}^{N \times d}$, key $\mathbf{K} \in \mathbb{R}^{N \times d}$, and value $\mathbf{V} \in \mathbb{R}^{N \times d}$, the linear attention output is defined as:

$$\begin{aligned} O_i &= \sum_{j=1}^N \frac{\text{ReLU}(Q_i) \text{ReLU}(K_j)^\top V_j}{\sum_{j=1}^N \text{ReLU}(Q_i) \text{ReLU}(K_j)^\top} \\ &= \frac{\text{ReLU}(Q_i) \left(\sum_{j=1}^N \text{ReLU}(K_j)^\top V_j \right)}{\text{ReLU}(Q_i) \left(\sum_{j=1}^N \text{ReLU}(K_j)^\top \right)} \end{aligned} \quad (4)$$

Instead of computing attention weights for every query-key pair, the shared terms $\sum_{j=1}^N \text{ReLU}(K_j)^\top V_j \in \mathbb{R}^{d \times d}$ and $\sum_{j=1}^N \text{ReLU}(K_j)^\top \in \mathbb{R}^{d \times 1}$ are computed only once, resulting in a lightweight and effective Linear DiT Block.

Finally, we adopt a lightweight fusion strategy that concatenates shallow convolutional features with motion guidance and latent representations before processing by the Linear DiT block, effectively integrating complementary cues while preserving efficiency.



Figure 5. Qualitative comparison on GoPro, BSD, and RSBlur (From top to bottom). GLOWDeblur effectively handles diverse blur patterns with high-quality restorations.

Table 4. Quantitative comparison with SOTA deblur models across real-world datasets RWBI and RWBlur400. Higher values are better for \uparrow metrics, lower for \downarrow . Since these datasets lack ground-truth annotations, only no-reference metrics are reported.

Dataset	Metrics	Restormer[35]	Restormer*[35]	HI-Diff[6]	DiffIR[30]	MISC-Filter[14]	MLWNet[8]	FPro[41]	Diff-Plugin[15]	Ours
RWBI [36]	MANIQA [32] \uparrow	0.501	0.522	0.554	0.494	0.492	0.565	0.483	0.460	0.635
	LIQE [38] \uparrow	1.846	2.180	2.875	1.807	2.150	3.068	1.771	1.371	3.732
	NRQM [16] \uparrow	5.433	5.608	5.879	5.457	5.079	6.185	5.474	5.028	6.393
	CLIP-IQA [27] \uparrow	0.257	0.283	0.372	0.256	0.301	0.424	0.236	0.234	0.474
	PI [3] \downarrow	5.291	5.133	4.993	5.353	5.468	4.459	5.182	5.670	4.789
	BRISQUE [17] \downarrow	39.945	39.192	40.674	42.319	43.271	37.403	39.581	40.488	36.625
	NIQE [18] \downarrow	5.682	5.545	5.589	5.831	5.793	4.886	5.550	5.988	4.796
RWBlur400	ILNIQE [37] \downarrow	40.760	37.569	37.047	41.304	38.705	34.259	40.208	47.048	33.271
	MANIQA \uparrow	0.509	0.530	0.490	0.493	0.455	0.517	0.481	0.497	0.604
	LIQE \uparrow	1.746	1.893	2.041	1.983	1.780	2.136	1.844	1.808	2.390
	NRQM \uparrow	4.956	5.471	5.411	5.747	4.901	5.736	5.783	5.660	6.746
	CLIP-IQA \uparrow	0.333	0.352	0.367	0.339	0.305	0.362	0.313	0.360	0.459
	PI \downarrow	4.788	4.734	4.990	4.578	5.236	4.461	4.520	4.649	3.786
	BRISQUE \downarrow	41.083	40.620	43.704	34.578	46.365	41.043	31.025	30.259	27.956
RWBlur400	NIQE \downarrow	4.971	4.817	5.229	4.751	5.204	4.575	4.609	4.777	4.576
	ILNIQE \downarrow	31.732	31.796	34.968	32.232	34.699	32.491	32.749	33.989	29.809

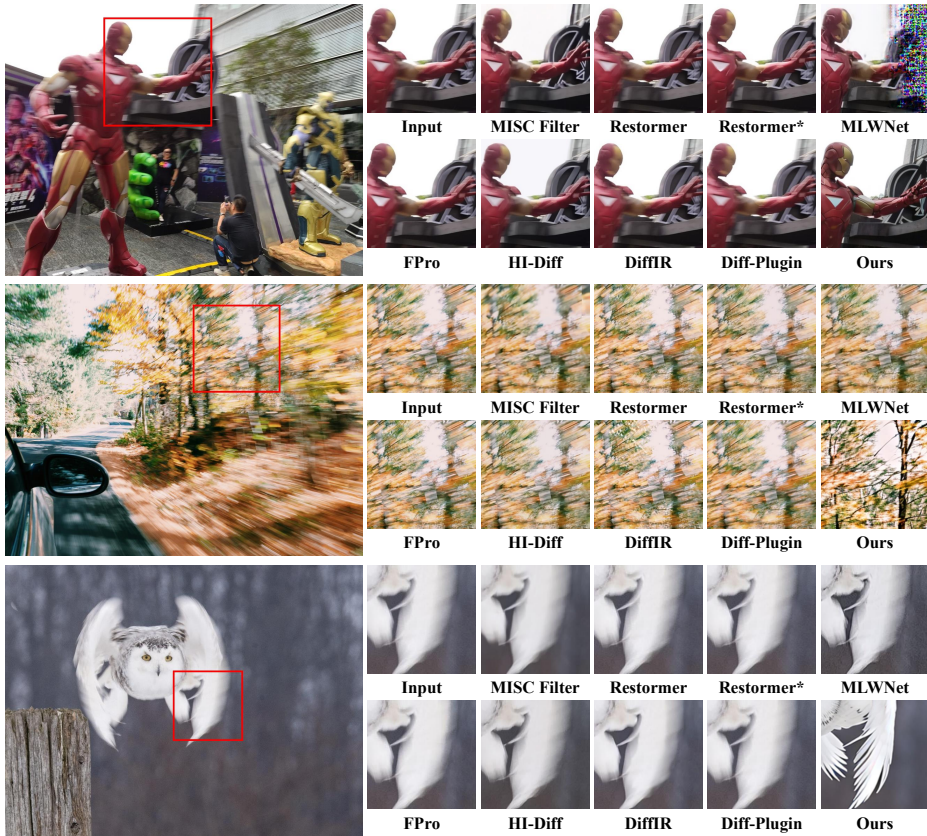


Figure 6. Comparison with SOTA deblur models on real-world datasets RWBI and RWBlur400.

4. Experiments

4.1. Experiment Settings

Training proceeds in two stages. First, BPP is performed on simulated datasets, including GSBlur (3D Gaussian Splatting with randomized camera trajectories) and an augmented subset of LSDIR [13] (by simply adding Gaussian and motion blur at different levels). Although less realistic, these datasets provide broad blur pattern coverage. Sec-

ond, we jointly fine-tune on GoPro, HIDE, REDS, Real-Blur, BSD, and RSBlur to align these priors with real-world distributions and enhance restoration quality. More implementation details are given in the Appendix Sec. 7.

We evaluate methods on six real-captured datasets for cross-dataset generalization. For real-world applicability, we further test on RWBI [36] and our collected RWBlur400. Distinguished from existing benchmarks that are limited to street views, RWBlur400 is widely collected

Table 5. Ablation studies on REDS and RSBlur. Gray indicates the settings of GLOWDeblur.

Dataset	No.	Model Modules			Data Pipeline		Metrics			
		$N_{\text{Pre-align}}$	G_{motion}	G_{text}	BPP	Mix all	MANIQA [32] \uparrow	LIQE [38] \uparrow	NRQM [16] \uparrow	BRISQUE [17] \downarrow
REDS [20]	(a)	\times	\times	\times	\checkmark	\times	0.565	1.817	5.968	34.297
	(b)	\checkmark	\times	\times	\checkmark	\times	0.605	2.099	6.250	32.230
	(c)	\checkmark	\checkmark	\times	\checkmark	\times	0.635	2.480	7.340	27.810
	(d)	\checkmark	\checkmark	\checkmark	\checkmark	\times	0.642	2.570	7.352	25.695
	(e)	\checkmark	\checkmark	\checkmark	\times	\checkmark	0.608	2.255	6.014	31.794
RSBlur [23]	(a)	\times	\times	\times	\checkmark	\times	0.463	1.132	4.392	43.854
	(b)	\checkmark	\times	\times	\checkmark	\times	0.484	1.181	4.715	39.940
	(c)	\checkmark	\checkmark	\times	\checkmark	\times	0.526	1.369	5.421	32.578
	(d)	\checkmark	\checkmark	\checkmark	\checkmark	\times	0.533	1.404	5.597	30.677
	(e)	\checkmark	\checkmark	\checkmark	\times	\checkmark	0.495	1.283	5.057	41.510

from the web, providing comprehensive coverage of diverse scene categories and complex blur patterns. Visual examples and detailed descriptions are provided in Appendix Sec. 11.1. Overall, we employ both reference-based and no-reference metrics to comprehensively evaluate deblurring performance. For reference-based evaluation, we use PSNR and SSIM. However, since recent image restoration research increasingly prioritizes perceptual quality over purely pixel-wise fidelity, our evaluation also places a strong emphasis on perceptual aspects. To this end, we adopt a diverse set of no-reference quality metrics—including MANIQA [32], LIQE [38], NRQM [16], CLIP-IQA [27], PI [3], BRISQUE [17], NIQE [18], and IL-NIQE [37], which together provide a thorough assessment of perceptual quality and better reflect real-world visual performance.

4.2. Comparisons with State of the Arts

We compare GLOWDeblur with state-of-the-art approaches from two categories. The first includes recent deblurring-specific methods such as HI-Diff, MISCFILTER, and ML-WNet. The second covers general restoration frameworks such as Restormer (and Restormer* retrained under our pipeline), DiffIR, FPro, and Diff-Plugin. Both categories contain a mix of diffusion-based and non-diffusion baselines, allowing a fair and comprehensive evaluation.

4.2.1. Cross-Dataset Generalization

We evaluate cross-dataset generalization on six widely used datasets. As shown in Figure 3, GLOWDeblur mitigates cross-dataset distribution gaps, achieving strong deblurring performance and high-quality restoration with competitive fidelity. Restormer* also achieves good fidelity across different datasets. Figure 5 provides qualitative comparisons, with additional results presented in Appendix Sec. 11. These results demonstrate that GLOWDeblur robustly handles complex blur patterns and produces high-quality restorations. More results are provided in the Appendix Sec. 11.

4.2.2. Real-World Evaluation

We evaluate real-world performance on RWBI and collected RWBlur400 datasets. As shown in Table. 4, GLOWDeblur consistently outperforms state-of-the-art baselines, demonstrating superior performance under real-world degradations. Restormer* also achieves significant improvements compared to its original version. Figure. 6 presents qualitative comparisons, where existing methods fail under severe blur, but GLOWDeblur produces clear and reliable restorations in real-world scenarios. More results are provided in the Appendix Sec. 11.

4.3. Ablation Studies

We conduct ablation studies on REDS and RSBlur (Table. 5). The Pre-Reconstruction & Domain-Alignment module provides consistent gains (a,b) by stabilizing representations and easing the diffusion backbone. Motion guidance enhances blur priors with trajectory cues (b,c), while semantic guidance introduces high-level semantics to recover severely degraded regions (c,d). Replacing BPP with naïve mixed-data training causes clear drops (d,e), confirming its role in bridging cross-dataset gaps. Overall, these results validate the effectiveness of both BPP and the model components. Qualitative results of motion guidance and semantic guidance are provided in the Appendix Sec. 9.

5. Conclusion

In this work, we identify blur pattern diversity as key to generalization and propose GLOWDeblur, a lightweight diffusion-based framework that integrates Blur Pattern Pre-training (BPP) and Motion & Semantic Guidance (MoSeG), achieving state-of-the-art performance on multiple synthetic and real-world datasets with substantially stronger generalization.

References

[1] Yuang Ai, Xiaoqiang Zhou, Huaibo Huang, Xiaotian Han, Zhengyu Chen, Quanzeng You, and Hongxia Yang. Dream-clear: High-capacity real-world image restoration with privacy-safe dataset curation. *Advances in Neural Information Processing Systems*, 37:55443–55469, 2024. 2, 3

[2] Shuai Bai, Keqin Chen, Xuejing Liu, Jialin Wang, Wenbin Ge, Sibo Song, Kai Dang, Peng Wang, Shijie Wang, Jun Tang, Humen Zhong, Yuanzhi Zhu, Mingkun Yang, Zhao-hai Li, Jianqiang Wan, Pengfei Wang, Wei Ding, Zheren Fu, Yiheng Xu, Jiabo Ye, Xi Zhang, Tianbao Xie, Zesen Cheng, Hang Zhang, Zhibo Yang, Haiyang Xu, and Junyang Lin. Qwen2.5-vl technical report. *arXiv preprint arXiv:2502.13923*, 2025. 5

[3] Yochai Blau, Roey Mechrez, Radu Timofte, Tomer Michaeli, and Lihi Zelnik-Manor. The 2018 pirm challenge on perceptual image super-resolution. In *Proceedings of the European conference on computer vision (ECCV) workshops*, pages 0–0, 2018. 6, 8, 9

[4] Shuo Cao, Nan Ma, Jiayang Li, Xiaohui Li, Lihao Shao, Kaiwen Zhu, Yu Zhou, Yuandong Pu, Jiarui Wu, Jiaquan Wang, Bo Qu, Wenhui Wang, Yu Qiao, Dajun Yao, and Yihao Liu. Artimuse: Fine-grained image aesthetics assessment with joint scoring and expert-level understanding, 2025. 3

[5] Liangyu Chen, Xiaojie Chu, Xiangyu Zhang, and Jian Sun. Simple baselines for image restoration. In *European conference on computer vision*, pages 17–33. Springer, 2022. 6

[6] Zheng Chen, Yulun Zhang, Ding Liu, Jinjin Gu, Linghe Kong, Xin Yuan, et al. Hierarchical integration diffusion model for realistic image deblurring. *Advances in neural information processing systems*, 36:29114–29125, 2023. 2, 6, 8, 1

[7] Patrick Esser, Sumith Kulal, Andreas Blattmann, Rahim Entezari, Jonas Müller, Harry Saini, Yam Levi, Dominik Lorenz, Axel Sauer, Frederic Boesel, et al. Scaling rectified flow transformers for high-resolution image synthesis. In *Forty-first international conference on machine learning*, 2024. 2, 3

[8] Xin Gao, Tianheng Qiu, Xinyu Zhang, Hanlin Bai, Kang Liu, Xuan Huang, Hu Wei, Guoying Zhang, and Huaping Liu. Efficient multi-scale network with learnable discrete wavelet transform for blind motion deblurring. In *Proceedings of the IEEE/CVF Conference on Computer Vision and Pattern Recognition*, pages 2733–2742, 2024. 2, 6, 8, 1

[9] Jonathan Ho, Ajay Jain, and Pieter Abbeel. Denoising diffusion probabilistic models. *Advances in neural information processing systems*, 33:6840–6851, 2020. 2

[10] Dilip Krishnan, Terence Tay, and Rob Fergus. Blind deconvolution using a normalized sparsity measure. In *CVPR 2011*, pages 233–240, 2011. 1

[11] Dongwoo Lee, Joonkyu Park, and Kyoung Mu Lee. Gs-blur: A 3d scene-based dataset for realistic image deblurring, 2024. 2, 3, 1

[12] Xiaohui Li, Shaobin Zhuang, Shuo Cao, Yang Yang, Yuan-dong Pu, Qi Qin, Siqi Luo, Bin Fu, and Yihao Liu. Lin-earsr: Unlocking linear attention for stable and efficient image super-resolution. *arXiv preprint arXiv:2501.01234*, 2025. 3, 6, 2

[13] Yawei Li, Kai Zhang, Jingyun Liang, Jiezhang Cao, Ce Liu, Rui Gong, Yulun Zhang, Hao Tang, Yun Liu, Denis Deman-dolx, et al. Lsdir: A large scale dataset for image restoration. In *Proceedings of the IEEE/CVF Conference on Computer Vision and Pattern Recognition*, pages 1775–1787, 2023. 8

[14] Chengxu Liu, Xuan Wang, Xiangyu Xu, Ruhao Tian, Shuai Li, Xueming Qian, and Ming-Hsuan Yang. Motion-adaptive separable collaborative filters for blind motion deblurring. In *Proceedings of the IEEE/CVF Conference on Computer Vision and Pattern Recognition*, pages 25595–25605, 2024. 2, 6, 8, 1

[15] Yuhao Liu, Zhanghan Ke, Fang Liu, Nanxuan Zhao, and Rynson WH Lau. Diff-plugin: Revitalizing details for diffusion-based low-level tasks. In *Proceedings of the IEEE/CVF Conference on Computer Vision and Pattern Recognition*, pages 4197–4208, 2024. 2, 6, 8, 1

[16] Chao Ma, Chih-Yuan Yang, Xiaokang Yang, and Ming-Hsuan Yang. Learning a no-reference quality metric for single-image super-resolution. *Computer Vision and Image Understanding*, 158:1–16, 2017. 6, 8, 9

[17] Anish Mittal, Anush K. Moorthy, and Alan C. Bovik. Blind/referenceless image spatial quality evaluator. In *2011 Conference Record of the Forty Fifth Asilomar Conference on Signals, Systems and Computers (ASILOMAR)*, pages 723–727, 2011. 6, 8, 9

[18] Anish Mittal, Rajiv Soundararajan, and Alan C. Bovik. Making a “completely blind” image quality analyzer. *IEEE Signal Processing Letters*, 20(3):209–212, 2013. 6, 8, 9

[19] Seungjun Nah, Tae Hyun Kim, and Kyoung Mu Lee. Deep multi-scale convolutional neural network for dynamic scene deblurring. In *Proceedings of the IEEE conference on computer vision and pattern recognition*, pages 3883–3891, 2017. 2, 3, 6, 1, 8

[20] Seungjun Nah, Sungyong Baik, Seokil Hong, Gyeongsik Moon, Sanghyun Son, Radu Timofte, and Kyoung Mu Lee. Ntire 2019 challenge on video deblurring and super-resolution: Dataset and study. In *Proceedings of the IEEE/CVF conference on computer vision and pattern recognition workshops*, pages 0–0, 2019. 2, 3, 6, 9, 1, 8

[21] Jinshan Pan, Deqing Sun, Hanspeter Pfister, and Ming-Hsuan Yang. Blind image deblurring using dark channel prior. In *2016 IEEE Conference on Computer Vision and Pattern Recognition (CVPR)*, pages 1628–1636, 2016. 1

[22] Jaesung Rim, Haeyun Lee, Jucheol Won, and Sunghyun Cho. Real-world blur dataset for learning and benchmarking deblurring algorithms. In *European conference on computer vision*, pages 184–201. Springer, 2020. 2, 3, 5, 6, 1, 8

[23] Jaesung Rim, Geonung Kim, Jungeon Kim, Junyoung Lee, Seungyong Lee, and Sunghyun Cho. Realistic blur synthesis for learning image deblurring. In *European conference on computer vision*, pages 487–503. Springer, 2022. 2, 3, 5, 6, 9, 1, 8

[24] Robin Rombach, Andreas Blattmann, Dominik Lorenz, Patrick Esser, and Björn Ommer. High-resolution image synthesis with latent diffusion models. In *Proceedings of*

the IEEE/CVF conference on computer vision and pattern recognition, pages 10684–10695, 2022. 2

[25] Ziyi Shen, Wenguan Wang, Xiankai Lu, Jianbing Shen, Haibin Ling, Tingfa Xu, and Ling Shao. Human-aware motion deblurring. In *Proceedings of the IEEE/CVF international conference on computer vision*, pages 5572–5581, 2019. 2, 3, 6, 1, 8

[26] Fu-Jen Tsai, Yan-Tsung Peng, Yen-Yu Lin, Chung-Chi Tsai, and Chia-Wen Lin. Stripformer: Strip transformer for fast image deblurring. In *European conference on computer vision*, pages 146–162. Springer, 2022. 1

[27] Jianyi Wang, Kelvin CK Chan, and Chen Change Loy. Exploring clip for assessing the look and feel of images. In *AAAI*, 2023. 6, 8, 9

[28] Zhendong Wang, Xiaodong Cun, Jianmin Bao, Wengang Zhou, Jianzhuang Liu, and Houqiang Li. Uformer: A general u-shaped transformer for image restoration. In *Proceedings of the IEEE/CVF conference on computer vision and pattern recognition*, pages 17683–17693, 2022. 1

[29] Jia-Hao Wu, Fu-Jen Tsai, Yan-Tsung Peng, Chung-Chi Tsai, Chia-Wen Lin, and Yen-Yu Lin. Id-blau: Image deblurring by implicit diffusion-based reblurring augmentation. In *Proceedings of the IEEE/CVF Conference on Computer Vision and Pattern Recognition*, pages 25847–25856, 2024. 2

[30] Bin Xia, Yulun Zhang, Shiyin Wang, Yitong Wang, Xinglong Wu, Yapeng Tian, Wenming Yang, and Luc Van Gool. Diffir: Efficient diffusion model for image restoration. In *Proceedings of the IEEE/CVF international conference on computer vision*, pages 13095–13105, 2023. 2, 6, 8, 1

[31] Enze Xie, Junsong Chen, Junyu Chen, Han Cai, Haotian Tang, Yujun Lin, Zhekai Zhang, Muyang Li, Ligeng Zhu, Yao Lu, et al. Sana: Efficient high-resolution image synthesis with linear diffusion transformers. *arXiv preprint arXiv:2410.10629*, 2024. 6, 2

[32] Sidi Yang, Tianhe Wu, Shuwei Shi, Shanshan Lao, Yuan Gong, Mingdeng Cao, Jiahao Wang, and Yujiu Yang. Maniq: Multi-dimension attention network for no-reference image quality assessment. In *Proceedings of the IEEE/CVF conference on computer vision and pattern recognition*, pages 1191–1200, 2022. 6, 8, 9

[33] Zhiyuan You, Xin Cai, Jinjin Gu, Tianfan Xue, and Chao Dong. Teaching large language models to regress accurate image quality scores using score distribution. In *IEEE Conference on Computer Vision and Pattern Recognition*, 2025. 3

[34] Fanghua Yu, Jinjin Gu, Zheyuan Li, Jinfan Hu, Xiangtao Kong, Xintao Wang, Jingwen He, Yu Qiao, and Chao Dong. Scaling up to excellence: Practicing model scaling for photo-realistic image restoration in the wild. In *Proceedings of the IEEE/CVF conference on computer vision and pattern recognition*, pages 25669–25680, 2024. 3, 2

[35] Syed Waqas Zamir, Aditya Arora, Salman Khan, Munawar Hayat, Fahad Shahbaz Khan, and Ming-Hsuan Yang. Restormer: Efficient transformer for high-resolution image restoration. In *Proceedings of the IEEE/CVF conference on computer vision and pattern recognition*, pages 5728–5739, 2022. 2, 6, 8, 1

[36] Kaihao Zhang, Wenhan Luo, Yiran Zhong, Lin Ma, Bjorn Stenger, Wei Liu, and Hongdong Li. Deblurring by realistic blurring. In *Proceedings of the IEEE/CVF conference on computer vision and pattern recognition*, pages 2737–2746, 2020. 8

[37] Lin Zhang, Lei Zhang, and Alan C. Bovik. A feature-enriched completely blind image quality evaluator. *IEEE Transactions on Image Processing*, 24(8):2579–2591, 2015. 6, 8, 9

[38] Weixia Zhang, Guangtao Zhai, Ying Wei, Xiaokang Yang, and Kede Ma. Blind image quality assessment via vision-language correspondence: A multitask learning perspective. In *Proceedings of the IEEE/CVF conference on computer vision and pattern recognition*, pages 14071–14081, 2023. 6, 8, 9

[39] Youjian Zhang, Chaoyue Wang, Stephen J Maybank, and Dacheng Tao. Exposure trajectory recovery from motion blur. *IEEE Transactions on Pattern Analysis and Machine Intelligence*, 44(11):7490–7504, 2021. 5

[40] Zhihang Zhong, Ye Gao, Yingqiang Zheng, and Bo Zheng. Efficient spatio-temporal recurrent neural network for video deblurring. In *European conference on computer vision*, pages 191–207. Springer, 2020. 2, 3, 5, 6, 1

[41] Shihao Zhou, Jinshan Pan, Jinglei Shi, Duosheng Chen, Lishen Qu, and Jufeng Yang. Seeing the unseen: A frequency prompt guided transformer for image restoration. In *European Conference on Computer Vision*, pages 246–264. Springer, 2024. 2, 6, 8, 1

Toward Generalizable Deblurring: Leveraging Massive Blur Priors with Linear Attention for Real-World Scenarios

Toward Generalizable Deblurring: Leveraging Massive Blur Priors with Linear Attention for Real-World Scenarios

Supplementary Material

6. Related Works

6.1. Image Deblurring

Image deblurring has long been a fundamental problem in low-level vision. Earlier methods mainly relied on hand-crafted priors and optimization-based formulations, such as gradient sparsity, edge sharpness, or statistical constraints [10, 21]. While these approaches provided valuable insights, their strong reliance on manually designed assumptions made them inadequate for handling complex and diverse real-world blur. With the rise of deep learning, researchers have shifted toward data-driven architectures, enabling significant improvements in both restoration quality and efficiency. In this work, we focus on the latest generation of learning-based approaches that have recently achieved state-of-the-art performance in deblurring and general image restoration.

Task-specific deblurring architectures [6, 8, 14, 26] have been extensively explored. Non-diffusion approaches introduce specialized designs tailored for motion blur removal. [26] employs directional strip-based attention to capture region-specific blur orientations and magnitudes efficiently. [14] leverages motion-adaptive collaborative filtering to handle spatially variant motion in real-world settings. [8] integrates multi-scale prediction with learnable wavelet transforms to preserve frequency and directional continuity. On the diffusion side, [6] designs a compact latent diffusion model with hierarchical integration to generate blur-aware priors for regression-based restoration. These specialized models typically achieve strong performance in blur removal but often generalize poorly when facing unseen blur patterns.

Beyond specialized models, general-purpose restoration frameworks [15, 28, 30, 35, 41] have also been widely applied to deblurring. Non-diffusion methods demonstrate strong versatility across tasks. [28] employs locally enhanced window attention to scale to high-resolution restoration, [35] introduces channel-wise self-attention for efficient global context modeling, and [41] incorporates frequency prompting to guide restoration across different degradations. Diffusion-based methods [15, 30] further extend general restoration: [30] integrates compact priors into efficient denoising diffusion, and [15] introduces lightweight task-specific plugin modules to adapt pre-trained diffusion models across diverse low-level vision tasks. Compared with task-specific designs, these general frameworks exhibit stronger cross-task robustness and gen-

eralization, though they often lag behind specialized models in task-optimized fidelity.

Despite these advances, most existing approaches still struggle with generalization in real-world scenarios. While task-specific methods achieve strong performance under their training distributions, they often fail to transfer across diverse blur patterns. General-purpose frameworks, though more robust across degradations, tend to sacrifice task-optimized fidelity. Overall, systematic investigation into real-world generalization for deblurring remains limited, leaving a critical gap that our work aims to address.

6.2. Deblurring Datasets

Progress in image deblurring has been closely tied to the availability of datasets. Yet, constructing suitable datasets is inherently challenging, as it involves balancing realism, diversity, and scalability. Synthetic datasets [19, 20, 25] such as GoPro [19], HIDE [25], and REDS [20] have been the dominant benchmarks for years. They are generated through pipelines that average or interpolate high-frame-rate videos to simulate camera exposure, offering large-scale paired data at relatively low cost. Such datasets have enabled rapid progress by providing standardized benchmarks, but the blur they simulate often deviates from real imaging processes. As a result, models trained on synthetic data may perform well in-distribution but fail to capture the irregular, spatially variant blur patterns observed in the wild.

To reduce this gap, real-captured datasets [22, 23, 40] have been developed. RealBlur [22], BSD [40], and RSBur [23] adopt specialized imaging systems—such as beam-splitter setups or synchronized multi-camera rigs—to capture geometrically aligned pairs of blurred and sharp images. These datasets provide authentic motion and defocus blur, more faithfully reflecting the complexity of real-world degradations. However, the hardware cost and collection complexity are significant, limiting the dataset scale and diversity. Even with substantial effort, it remains nearly impossible to comprehensively cover the range of blur magnitudes, orientations, and scene dynamics encountered in real scenarios.

Recently, simulation-based datasets such as GSBlur [11] have been proposed to improve diversity and controllability. By reconstructing 3D scenes with Gaussian Splatting and rendering them under randomized camera trajectories, GSBlur generates blur patterns beyond traditional frame-averaging pipelines. While this controllability broadens the degradation space, simulated blur still lacks the photometric

and structural fidelity of real imaging, leaving a clear gap to real-captured datasets.

In summary, synthetic datasets are abundant but unrealistic, real-captured ones are authentic but costly and narrow, and simulation-based ones offer diversity but lack realism. No dataset achieves both scale and fidelity, creating distribution gaps that cause models to overfit specific blur patterns and degrade sharply under unseen conditions. This underscores the need for strategies that explicitly address blur diversity and distribution mismatch, motivating our work.

6.3. Diffusion Models

Diffusion Models (DMs) [7, 9, 24] have recently emerged as powerful generative priors, synthesizing data from Gaussian noise through iterative denoising. Their success in image generation has inspired a series of applications in deblurring. In the context of deblurring, DiffIR [30] and HI-Diff [6] adopt diffusion-based priors with a two-stage training strategy to better capture blur statistics. More recently, IDBlau [29] leverages implicit diffusion to augment blur patterns under controllable settings, effectively enriching training data for downstream deblurring models.

Despite their effectiveness, most of these approaches remain computationally expensive. Large-scale pretrained diffusion models [1, 7, 34] possess billions of parameters, which, while offering strong generative priors, impose prohibitive training and inference costs that limit deployment in real-world scenarios like autonomous driving and mobile imaging. This challenge has motivated efforts to develop lightweight alternatives. For example, [31] proposes a linear-attention-based diffusion transformer that achieves high efficiency without sacrificing quality, demonstrating that architectural re-design and aggressive compression can bring diffusion models closer to practical deployment. Similarly, [12] and related works explore simplified diffusion formulations tailored for image restoration. Nonetheless, the exploration of lightweight diffusion for deblurring remains limited, leaving an open question of how to balance generalization, restoration fidelity, and efficiency under real-world constraints.

7. Implementation Details

Our model is trained in two stages. First, Blur Pattern Pre-training (BPP) is performed for 10k iterations on a synthetic mixture of GSBlur and an augmented subset of LS-DIR, where Gaussian and motion blur of varying levels are added to enrich pattern diversity. The model is then fine-tuned until convergence on a combined real-captured dataset including GoPro, HIDE, REDS, RealBlur, BSD, and RSBlur, aligning the learned priors with real-world distributions. Training is conducted using the Adam optimizer with an initial learning rate of 1e-4 and a batch size of 12x8.

All experiments are implemented in PyTorch and run on 8 NVIDIA A800 GPUs (80GB each).

8. Comprehensive Efficiency Gains from Our Lightweight Improvements

To meet the stringent efficiency demands of real-world deblurring deployment, our lightweight Pre-Aligned Linear Diffusion framework is specifically designed to address the common limitations of classical diffusion models such as large parameter counts and slow inference, as reflected in SDXL and FLUX-dev. By employing a 32x Deep Compression AutoEncoder to substantially reduce the number of latent tokens, and adopting a Linear DiT that replaces quadratic attention with an O(N) linear variant, our approach effectively removes the major computational bottlenecks found in existing diffusion systems. This lightweight design enables near-linear scaling on high-resolution inputs, which is crucial for real-time deblurring scenarios including mobile photography, online services, and embedded vision applications.

As shown in Table 6, our method achieves the highest throughput, the lowest latency, and the smallest parameter footprint, demonstrating that the linear-attention-based architecture provides a practical and highly efficient alternative to traditional diffusion frameworks.

Table 6. Comparison of Throughput, Latency, and Model Parameters

Methods	Throughput (\uparrow) (Samples/s)	Latency (\downarrow) (s/Sample)	Params (\downarrow) (B)
FLUX-dev	0.09	11.0	12.0
SDXL	0.3	3.3	2.6
Ours	1.7	0.6	1.6

9. Qualitative Results of Motion Guidance and Semantic Guidance



Figure 7. Qualitative results of motion guidance.

To visualize the effectiveness of our motion-aware design, we divide each input image into a 10×10 grid of patches and estimate the dominant motion direction within each patch. The aggregated patch-wise motion vectors are then rendered as line segments over the image, providing an intuitive qualitative representation of the underlying blur field. As shown in 7, our motion guidance accurately captures both the direction and the approximate magnitude of the local blur, even in scenes with spatially varying or non-uniform motion. The recovered motion structure exhibits a strong correspondence to the true blur patterns, revealing clear, coherent streak orientations that align with the motion that produced the blur.

Such explicit motion cues offer the model reliable, localized information about how the image was degraded. This strengthens the role of blur pattern awareness in the restoration process and allows the network to better adapt to complex motion distributions, ultimately enabling more faithful recovery compared with variants lacking motion guidance.

Beyond low-level motion cues, our semantic guidance (SeG) introduces high-level structural priors through text captions, which is particularly beneficial when restoring regions that suffer from severe degradation. As illustrated in Fig. 9, when the input image is heavily blurred, the visual evidence alone provides insufficient information for accurate reconstruction. In contrast, the semantic description—containing explicit references such as “Sydney Opera House at night” and the “prominent sail-shaped roofs”—offers strong contextual constraints that guide the model toward plausible structural recovery. These semantic cues enable the network to better infer the global architecture and restore fine details that would otherwise be ir-

retrievable. Consequently, SeG substantially enhances the model’s ability to handle severely blurred regions, yielding results with significantly improved clarity .

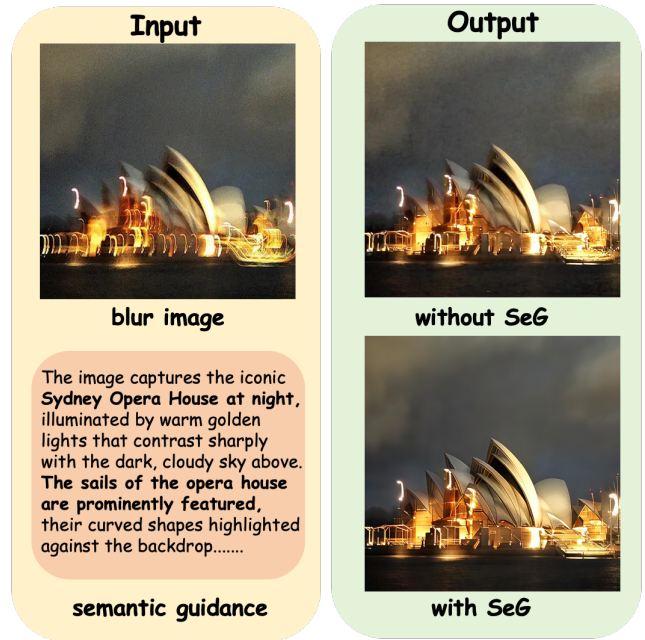


Figure 9. Qualitative results of semantic guidance.

10. Exploratory Comparison with Large-Scale General-Purpose Restoration Models

With the rapid development of diffusion models, large-scale variants trained on massive datasets have demonstrated impressive capabilities across diverse image restoration tasks [1, 7, 34]. These models, equipped with hundreds of millions or even billions of parameters, form the backbone of several general-purpose restoration frameworks that achieve state-of-the-art results in super-resolution, denoising, and image quality enhancement. Motivated by their success, we further investigate whether such models can leverage their scale and training data to generalize to real-world deblurring.

However, our experiments reveal notable limitations. Using SUPIR [34] as a representative model, we find that while it excels in enhancing perceptual quality—sometimes even surpassing ground-truth images in conventional quality metrics—it fails to effectively handle blur. As shown in 8, SUPIR struggles even on GoPro, one of the simplest synthetic benchmarks for motion deblurring, producing visually sharp but still blurred outputs. More strikingly, Figure. 10 also illustrates its shortcomings on complex real-world blur, where artifacts and residual degradation remain prominent.

These observations highlight an important gap: despite



Figure 8. Qualitative and quantitative comparison of SUPIR and GT on GoPro, showing quality scores exceeding GT but failure to remove blur.

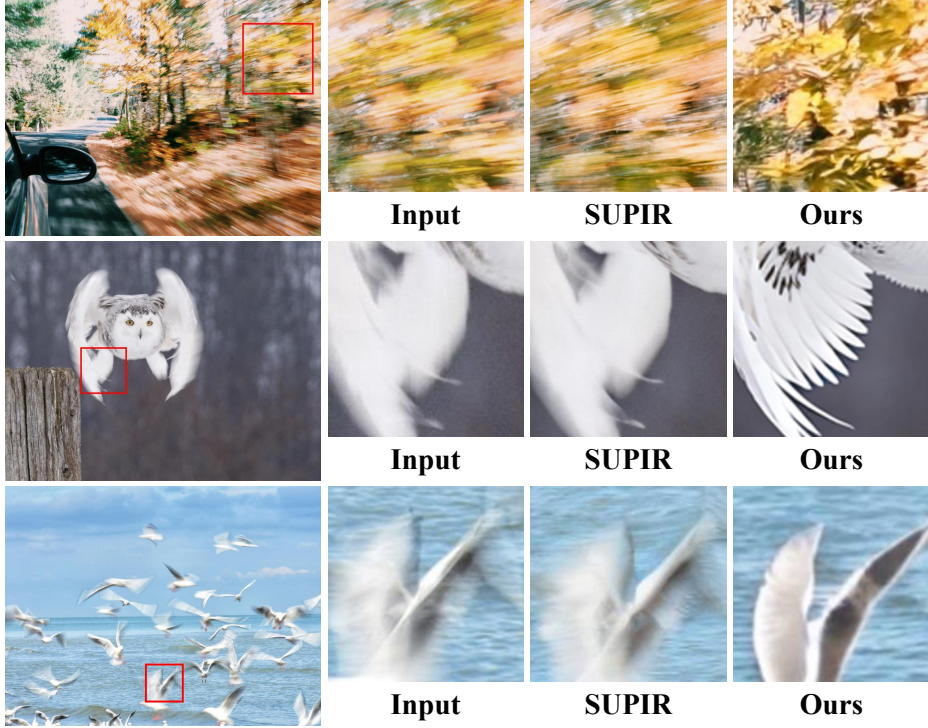


Figure 10. Quantitative comparison with SUPIR across real-world datasets.

their remarkable success in other restoration tasks, large-scale diffusion models are not inherently equipped to handle the structural complexity of blur. This contrast further validates the necessity of explicitly modeling blur priors, as pursued in our proposed framework, to achieve robust and

generalizable deblurring in real-world scenarios.

11. Additional Visual Results



Figure 11. Qualitative comparison on HIDE, Realblur, and REDS (From top to bottom). GLOWDeblur effectively handles diverse blur patterns with high-quality restorations.

To provide a more comprehensive assessment of our proposed method, we present additional visual results in this section, focusing on both cross-dataset generalization and real-world robustness.

First, to validate the generalization capability across different domains, Figure. 11 illustrates qualitative comparisons on three distinct datasets: HIDE, Realblur, and REDS (arranged from top to bottom). As observed, GLOWDeblur effectively handles diverse blur patterns—ranging from camera shake to complex object motion—and restores fine-

grained details with high fidelity, surpassing competing methods.

Furthermore, we extend our evaluation to challenging real-world scenarios. Figure. 12 and Figure. 13 provide extensive comparisons with state-of-the-art methods. In these cases, where degradations are severe and unpredictable, our model demonstrates superior robustness, consistently recovering sharp structures and legible text while suppressing common restoration artifacts.

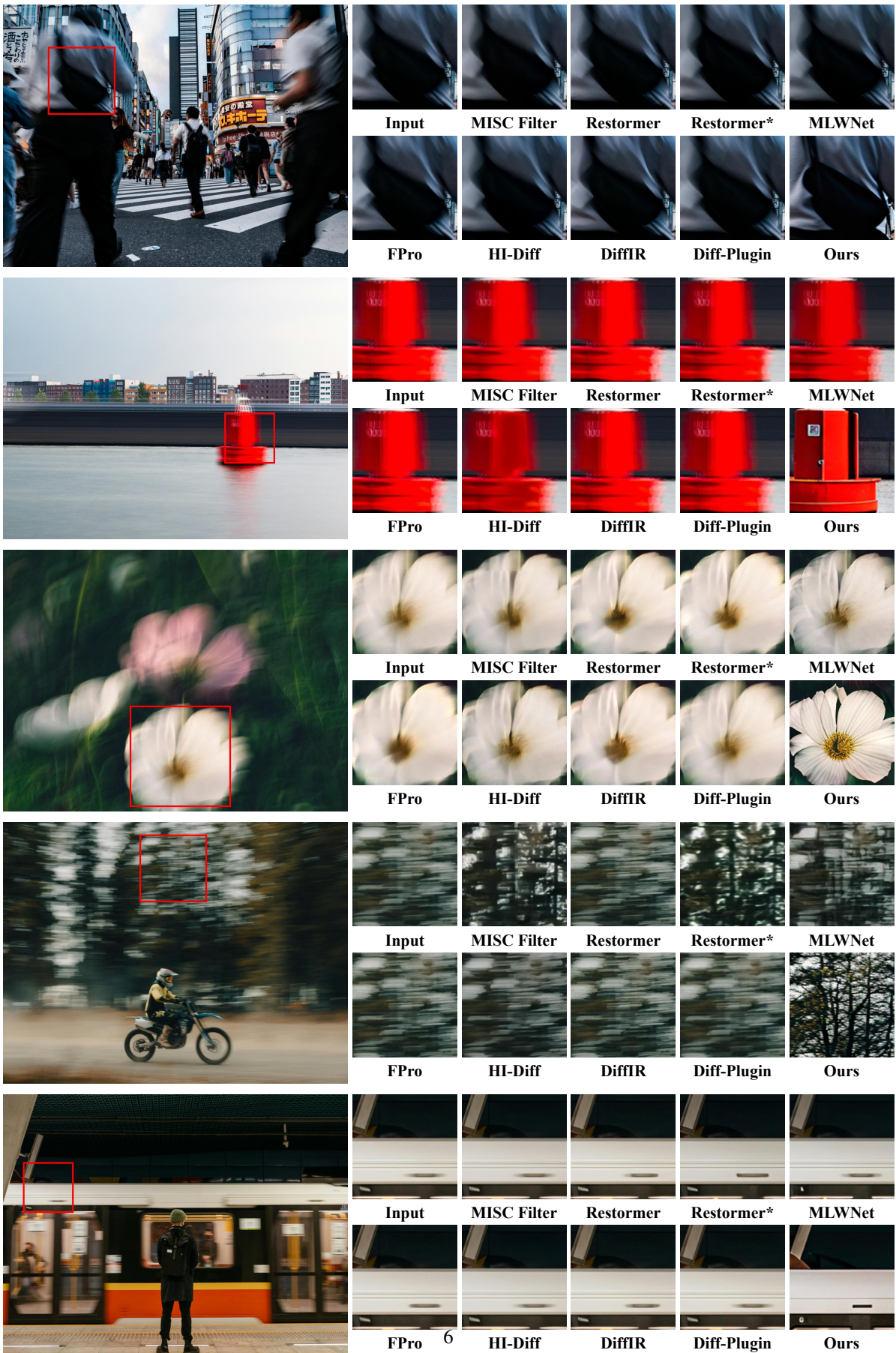


Figure 12. Comparison with SOTA deblur methods across real-world datasets.

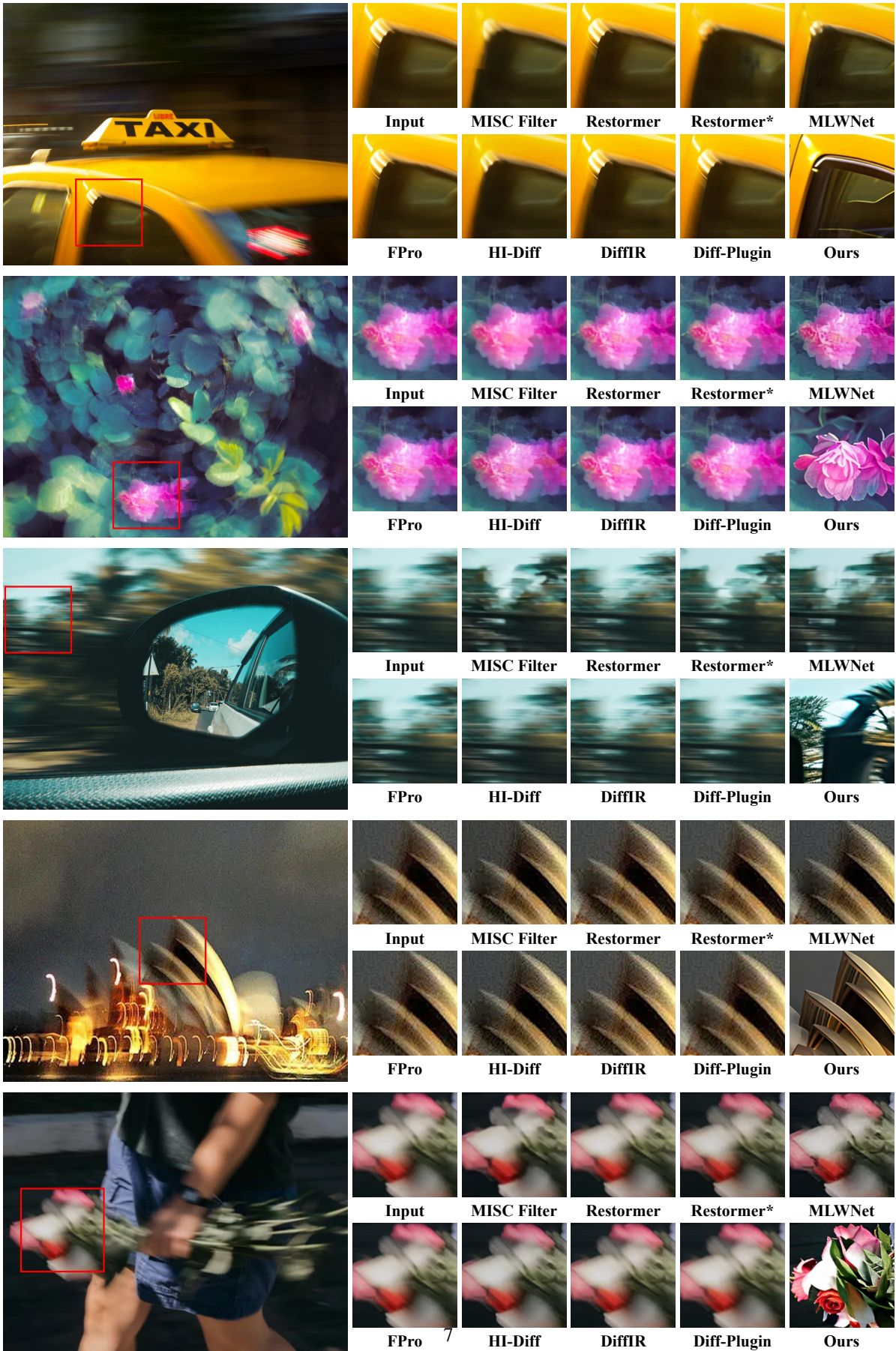


Figure 13. Comparison with SOTA deblur methods across real-world datasets.

11.1. RWBlur400

Existing motion deblurring datasets, such as GoPro [19], HIDE [25], RealBlur [22], REDS [20], and RSBlur [23], are predominantly captured in street environments. While valuable, they are inherently limited in their coverage of scene categories and blur patterns. Real-world blur, however, manifests in highly complex and diverse scenarios be-

yond street views. To address this gap and rigorously evaluate model generalization in the wild, we collected **RWBlur400**, a dataset comprising 400 diverse images sourced from the web. Unlike previous benchmarks, RWBlur400 encompasses a broad spectrum of subjects—ranging from views inside moving vehicles and dynamic wildlife to intricate flora—thereby posing a more realistic challenge. Representative examples are visualized in Figure 14.

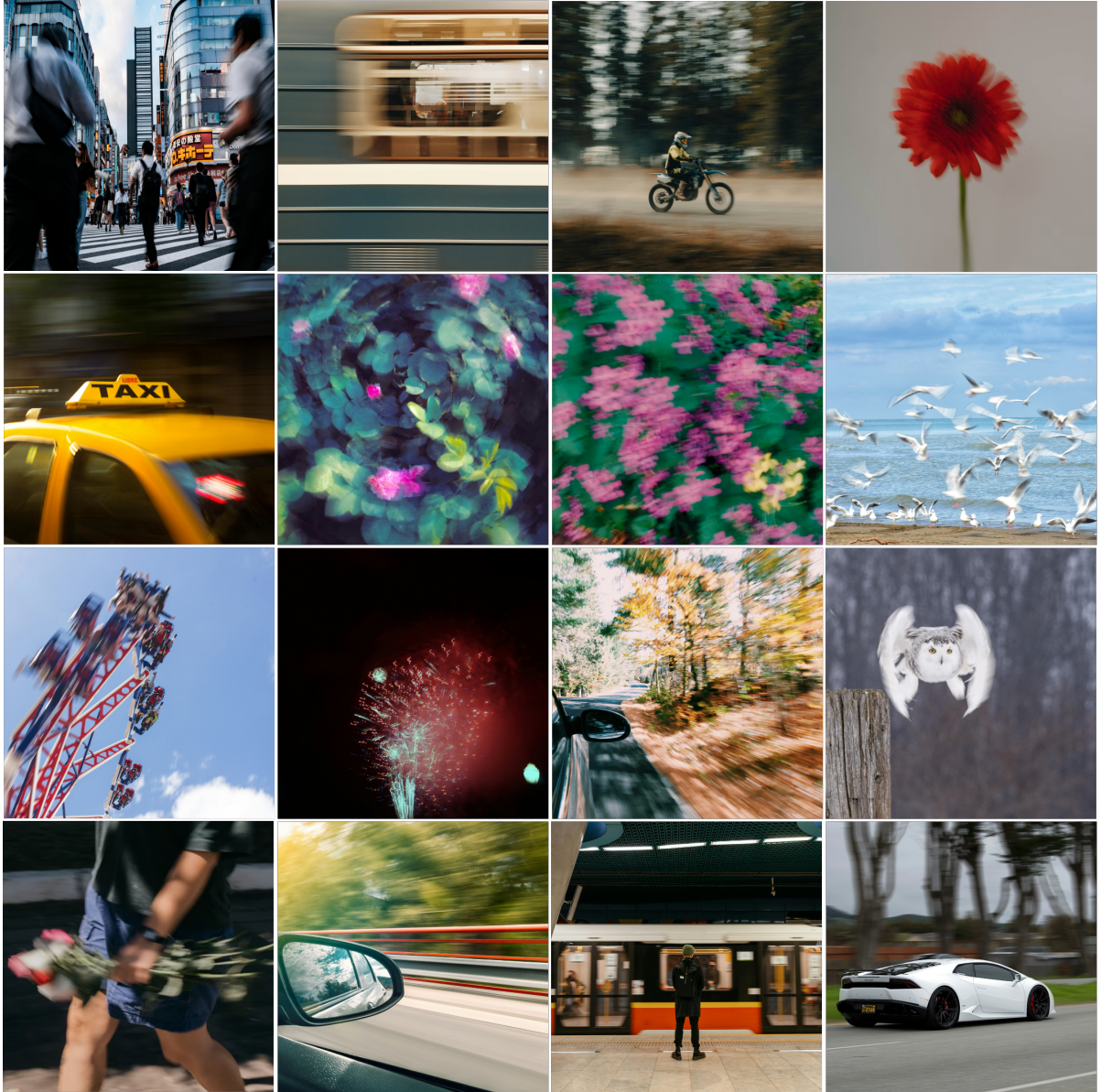


Figure 14. **Visual samples from the collected RWBlur400 dataset.** Unlike existing benchmarks that are predominantly limited to street views, RWBlur400 covers a wide spectrum of semantic scenarios (e.g., natural landscapes, animals, and night scenes) and diverse blur patterns (e.g., rapid object motion, camera shake, and light trails), reflecting complex degradations in the wild.